Dynamics of a polyelectrolyte in simple shear flow

Kandiledath Jayasree, Raj Kumar Manna, Debapriya Banerjee, and P. B. Sunil Kumar

Citation: The Journal of Chemical Physics **139**, 224902 (2013); doi: 10.1063/1.4837218
View online: http://dx.doi.org/10.1063/1.4837218
View Table of Contents: http://scitation.aip.org/content/aip/journal/jcp/139/22?ver=pdfcov
Published by the AIP Publishing

Dynamics of a polyelectrolyte in simple shear flow

Kandiledath Jayasree,[a] Raj Kumar Manna,[a] Debapriya Banerjee,[b] and P. B. Sunil Kumar[c]
Department of Physics, Indian Institute of Technology Madras, Chennai 600 036, India

(Received 13 July 2013; accepted 17 November 2013; published online 10 December 2013)

The configurational dynamics of a polyelectrolyte (PE), subjected to a simple shear flow, is studied using Brownian dynamics (BD) and Dissipative Particle Dynamics (DPD) simulations of a bead-spring model with explicit counterions. We explore the effect of counterion condensation on the tumbling and extension of PEs by varying the shear rates for a range of values of the electrostatic coupling parameter A (which is defined as the ratio of the Bjerrum length to the size of the monomer). In all cases, the power spectrum of $Rs(t)$ (which characterizes the projected length of the PE in the flow direction as a function of time) exhibits a power law decay at high frequencies, similar to that for a dumbbell in shear flow. For lower values of A ($A \sim 2$), the tumbling of the PE is periodic and is always associated with folding and stretching, which is in contrast to the oscillatory transition between the extended and globular states seen at higher values of A ($A \sim 15$). We observe that for $A \sim 2$ the tumbling frequency decreases and the average tumbling time increases with hydrodynamic interaction (HI). For $A > 15$, we observe a critical shear rate $\dot{\gamma}_c$ below which there is considerable counterion condensation and the PE remains in the globular state with a structure akin to that of a neutral polymer in poor solvent. The $\dot{\gamma}_c$ and the behavior of the PE above the critical shear rate are dependent on the HI. For a given shear rate, when there is considerable condensed counterion fluctuation, the PE extends as a whole and then collapses by the formation of folds with no observable periodicity in tumbling. When the condensed counterion fluctuations are suppressed, the polymer exhibits periodic tumbling. Simulation artifacts resulting from the implicit nature of the solvent and that due to boundary conditions are discussed by comparing the BD results with that obtained from the DPD simulations incorporating Ewald summation for electrostatics. © *2013 AIP Publishing LLC*. [http://dx.doi.org/10.1063/1.4837218]

I. INTRODUCTION

The response of polymers to a flow is relevant in understanding many natural processes and it has potential applications in various branches of biology and biophysics.[1,2] Most biopolymers, like DNA, RNA, proteins, etc., are polyelectrolytes (PEs) since they dissociate into charged macromolecules and counterions (CIs) in the presence of a polar solvent. Electrostatic interactions have significant effects on the physical properties of these polymers. Polyelectrolytes are highly sensitive to the environment as a small change in the interaction between ionized groups can change its structure into a great deal.[3,4] They exhibit a wide spectrum of conformations, which are controlled primarily by the solvent quality, salt concentration, and external fields.[5] Numerous studies have been conducted on the rheological properties of dilute polymer solutions in the presence of shear and elongational flow.[2] The properties of dilute PE solutions were also investigated using Brownian dynamics (BD) simulations.[6,7] Our aim is to analyze the configurational dynamics of a PE, for different electrostatic interaction strengths and taking all charge interactions explicitly, when subjected to a shear flow.

The recent surge of interest in single polymer conformations in shear flow was triggered by the success of experiments in tracking the dynamics of a single DNA molecule subjected to simple shear.[8,9] For shear flows with the Weissenberg number in the range of 0–80, an aperiodic end-over-end tumbling of the DNA was observed in these experiments. Following this, Hur *et al.*[10] carried out extensive numerical simulations of different models of neutral flexible polymers in a simple shear flow, which confirmed the aperiodic tumbling dynamics. In these studies, the polymer tumbling dynamics was analyzed using the power spectral density (PSD) of the polymer extension in the direction of flow and the tumbling time obtained directly from the end to end vector orientation. Later, evidence for periodic tumbling was obtained from a combination of single DNA molecule experiments and computer simulations, using the PSD of the polymer orientation angle.[11] More systematic investigations, at different environmental conditions, are required to get clearer picture of the behavior of DNA under shear. One of the parameters that was left out in these simulations was the stiffness of the polymer. Munk *et al.*[12] focused on this aspect and looked at the dynamics of semiflexible, charge-neutral polymers under shear using normal mode decomposition of continuous space curves. They reported that stiffness leads to periodic tumbling. Apart from DNA, the dynamics of a single protein molecule in shear flow conditions was also investigated using models that neglect all electrostatic interactions.

[a] K. Jayasree and R. K. Manna contributed equally to this work.
[b] Present address: Department of Materials Science and Engineering, University of Illinois, Urbana-Champaign, 1304 W. Green Street, Urbana, Illinois 61801, USA.
[c] Electronic mail: sunil@iitm.ac.in

Brownian dynamics simulation of a structure-based coarse-grained model was used to study two proteins ubiquitin and integrin.[13] This study suggested that the hydrodynamic interactions (HI) between amino acids hinder the unfolding of proteins and the unfolding is through a series of metastable intermediate states. Another protein that has been studied in great detail is the von Willebrand factor (vWF), a protein that is present in our circulatory system. The conformational dynamics of the vWF was investigated using a micro-fluidic device, and a reversible globule-stretch transition was observed.[14] In this context, the dynamics of a charge-neutral polymer, in poor solvent, in simple shear flow was studied using Brownian dynamics simulations in both the freely draining (FD) limit and with the inclusion of hydrodynamics.[15–17]

Since most of the biologically relevant macromolecules are charged, it is important to understand how electrostatic forces control the structure of these molecules in shear flows. This has fueled many simulations of charged polymers in shear flow.[6,18] The adsorption of a single PE in shear flow was looked into, using effective screened interactions between charges on the polymer backbone.[18] Note that the shear forces can also affect the charge distribution on the molecules by influencing the counterion condensation, and it is important to have all charged species represented explicitly. Such an approach was used to study the shear rheology of dilute PE solutions.[6] This study revealed that counterions play a relevant role in determining the properties like the solution viscosity.[6] Here, we use similar methods to study the conformational dynamics of a single polyelectrolyte in simple shear flow. The effects of shear rate, electrostatic interaction strength, and hydrodynamic interactions on the dynamics of the PE are analyzed. Depending on the strength of the electrostatic interaction and the solvent quality, the polyelectrolytes can assume different equilibrium conformations.[5] In good solvent conditions PE is known to exhibit, as a function of electrostatic interaction strength, three important conformations, (a) extended, (b) sausage, and (c) collapsed globular, which occur as the result of counterion condensation.[19,20] In this paper, we look at the effect of shear on some of these equilibrium conformations and show that the conformations and dynamics of the PE are determined by the number of counterions bound to it. The paper is organized as follows. In Sec. II, we describe the model and the details of the simulation procedure. In Sec. III, we present and discuss the results obtained from the simulations. In Sec. IV we compare the results from the BD simulations, in few cases, with Dissipative Particle Dynamics (DPD) simulations. We conclude in Sec. V with a short summary.

II. MODEL

We model the polyelectrolyte as a linear chain of N spherical beads of charge e and diameter b, connected through harmonic springs. The system is bounded within a cubic box of volume L^3. To ensure charge neutrality, we introduce N oppositely charged counterions, with the same valency and diameter as the backbone beads into the simulation box. We use two different simulation schemes to study the dynamics of this model PE in a shear flow. In the BD simulations, described in Subsection II A, the solvent effects are included implicitly through mobility matrices and a minimum image boundary condition is used for electrostatic interactions. The artifacts that may have resulted from these approximations are explicitly checked, in the regime of high electrostatic coupling, by DPD simulations that incorporate solvent explicitly and use Ewald summation for electrostatic interactions.

A. Brownian dynamics simulations

In this case the polymer dynamics is studied taking the solvent effects implicitly. The number density of beads in the simulation box is fixed as $10^{-4}/b^3$. A direct comparison to experimental charge density is not feasible in our model as we use coarse-grained description for the polymer but at the same time assume that counterions and monomers have the same size. A simple shear, with the flow in the x-direction and a velocity gradient $\dot{\gamma}$ in the z-direction, is imposed. The effect of the solvent, embedding the polyelectrolyte-counterion system, is included implicitly through the dielectric constant ϵ, a mobility matrix μ, and the disturbance matrix $\mathbf{C}$.[23] Shear can be imposed on the system in two different ways: (a) by imposing the Lees-Edwards boundary condition along the shear gradient direction[21] or (b) by giving a velocity $\pm(\dot{\gamma}L/2)\hat{e}_x$ to the hard walls placed at $z = 0$ and $z = L$. In case (a), periodic minimum image boundary conditions along the x, y, and z directions are used for all interactions, while in case (b), periodic minimum image boundary conditions are used along the x and y directions and a hard dielectric boundary condition (which neglects any image charge effects) along the z-direction. With these, the equation of motion for the ith bead (which can be a polyelectrolyte backbone or a counterion), at $\mathbf{r}_i$, in the over damped limit is[22,23]

$$\frac{d\mathbf{r}_i}{dt} = -\mu_{ij}\cdot\nabla_{\mathbf{r}_j}U + \nabla_{\mathbf{r}_j}\cdot\mathbf{D}_{ij} + \mathbf{v}(\mathbf{r_i}) + \mathbf{C}_i : \Upsilon + \sqrt{2k_BT}\mathbf{B}_{ij}\mathbf{f}_j(t), \quad (1)$$

where $\mathbf{v}(\mathbf{r}) = \dot{\gamma}z\hat{e}_x$ is the velocity field of the solvent, U is the total energy of the system, μ_{ij} is the component of the mobility tensor which incorporates the solvent-mediated hydrodynamic interaction between particles, $\mathbf{C}_i$ is the disturbance matrix which accounts for the contributions to the fluid velocity in the neighborhood of bead i due to the shear induced rotation of other beads in the system, and Υ is the velocity gradient tensor whose components are $\Upsilon_{\alpha\beta} = \dot{\gamma}\delta_{\alpha x}\delta_{\beta z}$. The third rank disturbance matrix $\mathbf{C}$ is given by

$$\mathbf{C}_i = -\frac{5}{2}\sum_{i\neq j}\left(\frac{a}{r_{ij}}\right)^3 \hat{\mathbf{r}}_{ij}\hat{\mathbf{r}}_{ij}\mathbf{r}_{ij}, \quad (2)$$

where $\mathbf{r}_{ij} = \mathbf{r}_i - \mathbf{r}_j$ and a is the radius of the bead. Since $\mathbf{C}_i$ decays as $1/r^2$, the most dominant solvent mediated interaction is the one through the mobility μ. Another point to note is that $\mathbf{C}_i$ is expected to be important when the beads can rotate freely and when they are sufficiently close to each other. Since individual monomers in a chain cannot rotate relative to each other, one expects the rotational coupling to be prominent only between the monomers and the CIs near it. It is also true that in real systems the counterions are generally

smaller than the monomers and a monomer counterion interaction through such a term will be negligible. These factors imply that the influence of the disturbance term on the PE dynamics, if any, can only be an artifact of the fact that we take all particles to have the same size. We tested this influence of $\mathbf{C}_i$ in our simulations and found it to be negligible.

When the Lees-Edwards boundary condition is used along the shear gradient direction, μ is given by the Rotne-Prager mobility tensor that accounts for the finite size of beads.[24] When hard walls are present in the shear gradient direction, we use the Rotne-Prager-Blake mobility tensor that accounts for the no-slip boundary condition on the walls and for the finite size of beads.[25,26] We find that the results obtained, using these two boundary conditions, are exactly the same. When hydrodynamic interactions are neglected, the disturbance tensor will be a null matrix, and the components of the mobility tensor take the simple form $\mu_{ij} = \mu_0\delta_{ij}$. Here $\mu_0 = 1/(6\pi\eta a)$ is the self-mobility of the beads with radius $a = b/2$; η is the solvent viscosity. $\mathbf{D} = k_BT\mu$ is the diffusion tensor. The term $\nabla_{\mathbf{r}_j} \cdot \mathbf{D}_{ij}$, in Eq. (1), implies drift of a particle caused by the gradient in the diffusion tensor. This term is exactly zero when the Rotne-Prager tensor is used. But in the presence of hard boundaries, where we use Rotne-Prager-Blake mobility tensor, self-mobility μ_{ii} of a particle is position dependent and thus the gradient in diffusion tensor is non-zero.[26] The last term on the right-hand side of Eq. (1) is the thermal noise, with components $f_{j\alpha}$ taken from a random distribution with zero mean and unit variance. The fluctuation dissipation theorem implies that the strength of the noise $\mathbf{B}$ satisfies the equation $\mu = \mathbf{B} \cdot \mathbf{B}^T$.[27] We obtained $\mathbf{B}$ using the Chebyshev polynomial approximation for the square root function,[28] and its accuracy was compared with the result obtained from the Cholesky decomposition.[29]

The total energy U of the system consists of three parts: (i) a purely repulsive Lennard-Jones potential (U_{LJ}) for the excluded volume given by

$$U_{LJ} = \epsilon_{LJ}\sum_{i<j}\left(\frac{b^{12}}{(\mathbf{r}_i - \mathbf{r}_j)^{12}} - \frac{2b^6}{(\mathbf{r}_i - \mathbf{r}_j)^6}\right) for\ |\mathbf{r}_i - \mathbf{r}_j| \le b,$$
$$U_{LJ} = 0\ for\ |\mathbf{r}_i - \mathbf{r}_j| > b, \tag{3}$$

(ii) the harmonic spring potential between the connected monomer beads is given by

$$U_{spring} = \sum_i k(|\mathbf{r_i} - \mathbf{r}_{i+1}| - b)^2, \tag{4}$$

with spring constant k; and (iii) the electrostatic potential between any pair of beads given by

$$U_c = Ak_BT\sum_{i<j}\frac{bs_is_j}{|\mathbf{r}_i - \mathbf{r}_j|}, \tag{5}$$

where s_i is the sign of the ion charge. The coupling strength $A = q^2l_B/b$ measures the ratio of the Coulomb to thermal energy of two beads at a separation b; here, q is the valency of the monomer, $l_B = e^2/4\pi\epsilon k_BT$ is the Bjerrum length, and e is the electronic charge. In addition, a short-range repulsive Lennard-Jones interaction between the walls and the beads was used whenever the hard wall boundary condition was used.

The equation of motion is made dimensionless by scaling the length, energy, time, and force variables by b, k_BT, $\tau = \tau_{BD} = b^2/\mu_0k_BT$, and k_BT/b, respectively. The parameters in the simulation, in these units, are $\epsilon_{LJ} = 1$ and $k = 800$. The stochastic differential equation is treated in the Ito interpretation. Thus, the discretized equation of motion in the scaled units can then be written as[17,29]

$$\tilde{r}_i(\tilde{t} + \delta\tilde{t}) = \tilde{r}_i(\tilde{t}) - \tilde{\mu}_{ij}\tilde{\nabla}_{r_j}\tilde{U}\delta\tilde{t} + \tilde{\nabla}_{r_j} \cdot \tilde{D}_{ij}\,\delta\tilde{t} + Pe\,\tilde{z}_i\,\delta\tilde{t} + \tilde{\mathbf{C}}_i : \tilde{\Upsilon}\delta\tilde{t} + \sqrt{2\delta\tilde{t}}\tilde{B}_{ij}\tilde{f}_j, \tag{6}$$

where, $Pe = \dot{\gamma}\tau$ is the Peclet number. The Weissenberg number is then defined as $Wi = Pe\,\tau_R\tau^{-1}$, where τ_R is the relaxation time of the PE in equilibrium. In our simulations, to obtain consistent results, we have used a time step $\delta\tilde{t} = 5 \times 10^{-5}\tau_{BD}$. The relaxation time τ_R is obtained from the PE end-to-end distance autocorrelation, in the absence of any external fields, for both the freely draining polyelectrolytes (BD-FD) and the polyelectrolytes in the presence of the hydrodynamic interactions (BD-HI) separately. Averages are obtained, for each set of parameters, over 10 different initial configurations. To obtain the power spectrum, each configuration is run for $2 \times 10^8\delta\tilde{t}$.

B. Dissipative particle dynamics simulations

For a finite PE, surrounded by counter ions, minimum image boundary conditions are expected to give reasonable results.[32,33] Similarly the effects of long range hydrodynamic interactions are expected to be reasonably well captured by the RP tensor. In order to check the effects of these approximations explicitly, we simulated a fully periodic system with Ewald method for electrostatic interactions in the presence of explicit solvent. The local momentum conservation was ensured using DPD thermostat.[38–40] The conservative interactions between polymer beads and the polymer and the counter ion beads are $\mathbf{F}_{ij}^{(C)} = -\nabla(U_{LJ} + U_{spring} + U_c)$ and are derived from the potentials given in Eqs. (3)–(5). Solvent is now included explicitly as DPD beads. The conservative force arising from the solvent-solvent, solvent-polymer, and solvent-counterion interaction is of soft repulsive nature and is given by $\mathbf{F}_{ij}^{(C)} = 25.0\omega(r_{ij})\mathbf{n}_{ij}$, where, $\mathbf{r}_{ij} = \mathbf{r}_j - \mathbf{r}_i$, $r_{ij} = |\mathbf{r}_{ij}|$, and $\mathbf{n}_{ij} = \mathbf{r}_{ij}/r_{ij}$. With b as the interactions cutoff radius, the weight factor is chosen as

$$\omega(r) = \begin{cases} 1 - r/b & \text{for } r \le b, \\ 0 & \text{for } r > b. \end{cases} \tag{7}$$

The choice of ω in Eq. (7) ensures that the solvent interactions are all soft and repulsive. The time evolution of the position and velocity of each DPD particle i, denoted by $(\mathbf{r}_i, \mathbf{v}_i)$, is governed by Hamilton's equations of motion. Apart from the above conservative forces there are dissipative ($\mathbf{F}_{ij}^{(D)}$) and random ($\mathbf{F}_{ij}^{(R)}$) pairwise thermostat forces acting between all pairs of particles. They are given by

$$\mathbf{F}_{ij}^{(D)} = \gamma_{ij}\omega^2(r_{ij})(\hat{\mathbf{r}}_{ij} \cdot \mathbf{v}_{ij})\mathbf{n}_{ij}, \tag{8}$$

$$\mathbf{F}_{ij}^{(R)} = \sigma_{ij}(\Delta t)^{-1/2}\omega(r_{ij})\theta_{ij}\mathbf{n}_{ij}, \tag{9}$$

where $\mathbf{v}_{ij} = \mathbf{v}_j - \mathbf{v}_i$ and θ_{ij} is a symmetric random variable satisfying

$$\langle \theta_{ij}(t) \rangle = 0, \tag{10}$$

$$\langle \theta_{ij}(t)\theta_{kl}(t') \rangle = (\delta_{ik}\delta_{jl} + \delta_{il}\delta_{jk})\delta(t - t'), \tag{11}$$

with $i \neq j$ and $k \neq l$. In Eq. (9), Δt is the iteration time step. The equations of motion of particle i are given by

$$d\mathbf{r}_i(t) = \mathbf{v}_i(t)dt, \tag{12}$$

$$m\, d\mathbf{v}_i(t) = \sum_j \left(\mathbf{F}_{ij}^{(C)}dt + \mathbf{F}_{ij}^{(D)}dt + \mathbf{F}_{ij}^{(R)}\sqrt{dt}\right), \tag{13}$$

where m is the mass of a single DPD particle. Here, for simplicity, masses of all types of DPD particles are taken to be equal. Constant temperature T implies that the parameters γ_{ij} and σ_{ij} in Eqs. (8) and (9) are related to each other by the fluctuation-dissipation theorem,

$$\gamma_{ij} = \sigma_{ij}^2/2k_{\mathrm{B}}T. \tag{14}$$

As in BD simulations, the equation of motion is made dimensionless by scaling the length, energy, and force variables by b, k_BT, and k_BT/b, respectively. Time is now scaled by $\tau_{DPD} = b\sqrt{(m/k_BT)}$. The simulation package LAMMPS[34] is used with Lees-Edwards boundary conditions for imposing the shear flow. We use two different boundary conditions for the electrostatic interactions, one through Ewald sum and another using periodic minimum image.

III. RESULTS AND DISCUSSIONS

Our interest here is to study the dynamics of a polyelectrolyte in a simple shear flow, for different values of the coupling constant A and shear rates. In good solvent conditions, different equilibrium conformational regimes obtained are (a) extended regime for $1 < A < 5$, (b) sausage regime $5 < A < 10$ and collapsed regime $A > 10$[19,20] (see Fig. 1). We, therefore, choose $A = 2$, 5, 10, and 20 to check the effects of shear on its conformational dynamics. The main feature that distinguishes the dynamics of PE under shear from that of a neutral polymer is the counterion fluctuation, which is significant for

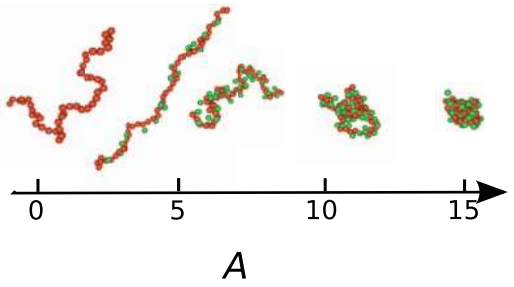

FIG. 1. A state diagram showing the equilibrium conformations of a polyelectrolyte in good solvent regime as a function of A. When $A = 0$, PE behaves like a self-avoiding random walk. As A increases PE shows different regimes: extended, sausage, and collapsed. Monomers are shown in red color and condensed counterions are shown in green color.[19]

$A < 15$. The HI, which suppress fluctuation in the number of condensed counterions (CCIs) through forces that tend to reduce the shear gradient between particles, play a significant role in determining the conformational dynamics of the PE in shear. We will come back to this point again later.

We compared the behavior of a PE with a particular parameter set using BD simulations and DPD simulations and found in general excellent agreement between the results obtained from these two methods at low A and will discuss only the BD results in this regime. However, we find that in the high A regime, the structure of the collapsed polymer and the arrangement of condensed counterions differ when the solvent is included explicitly, the main difference being a shift in the critical shear rate for extension of the PE. At the end of this section we will compare the results from BD and DPD in this regime.

A. Low electrostatic coupling, $A < 10$

When $A \sim 2$, the number of CCIs is small and the repulsion between like charged monomers keeps the PE stretched. Such a configuration tumbles, when placed in a shear flow. A typical sequence of configurations of a PE at $A = 2$ in a tumbling cycle is shown in the top panel of Fig. 2. The tumbling in this case is through the formation of a fold at one end proceeded by the movement of the two arms of the fold in

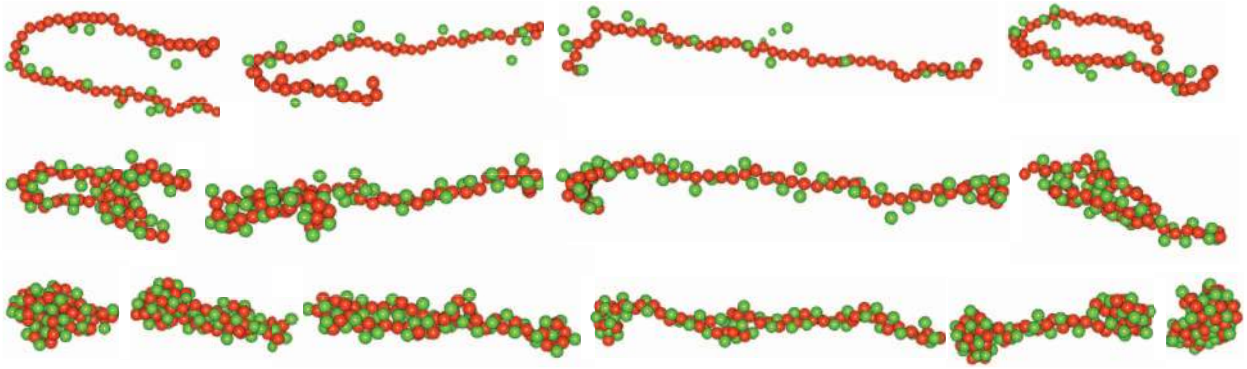

FIG. 2. Sequence of snap shots of an $N = 50$ BD-FD in a shear flow at $Wi = 20$ for different electrostatic coupling constants. Top panel: (from left) configurations of an $A = 2$ BD-FD at $\tilde{t} = 465$, $\tilde{t} = 472$, $\tilde{t} = 537$, and $\tilde{t} = 597$, respectively. Middle panel: (from left) configurations of an $A = 10$ BD-FD at $\tilde{t} = 587$, $\tilde{t} = 595$, $\tilde{t} = 657$, and $\tilde{t} = 682$. Bottom panel: (from left) configurations of an $A = 20$ BD-FD at $\tilde{t} = 935$, $\tilde{t} = 955$, $\tilde{t} = 962$, $\tilde{t} = 973$, $\tilde{t} = 990$, and $\tilde{t} = 995$. Only the polymer backbone (red color) and the condensed counterions (green color) are shown.

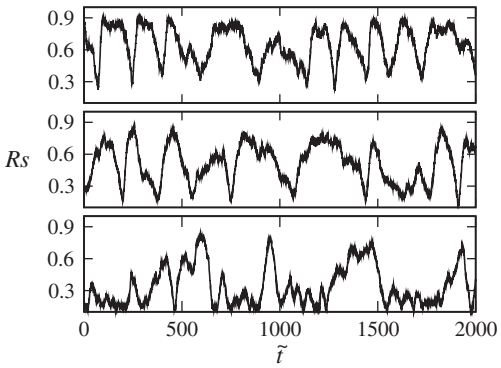

FIG. 3. Extension of an $N = 50$ BD-FD in the direction of flow as a function of time, at $Wi = 20$, for different coupling constants; $A = 2$ (top panel), $A = 10$ (middle panel), and $A = 20$ (bottom panel). The equilibrium conformations at these values of A are stretched, sausage like, and collapsed, respectively.

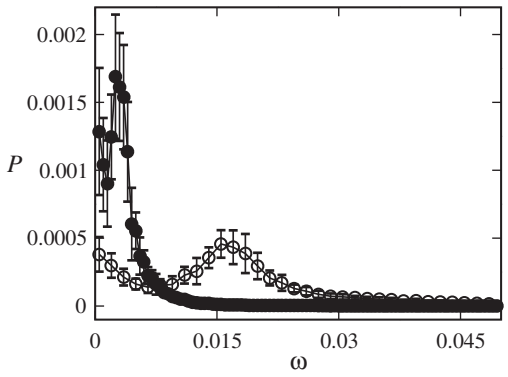

FIG. 5. Comparison of the power spectrum of the extension Rs of an $N = 50$, $A = 2$, BD-FD (filled circles), and BD-HI (open circles), in a shear flow at $Wi = 20$.

opposite directions. We have analyzed the tumbling dynamics using two methods: (a) time series of the PE extension, Rs, which is the ratio of projected length of the PE in the flow direction to the number of monomers N, and its power spectrum, (b) tracking the tumbling time from the orientation of the end to end vector.[35]

From the top panels of Figs. 2 and 3, which show the time series of Rs, it is evident that Rs has a propensity to stay closer to its maximum value at $A = 2$, implying an extended state of the PE. The sudden decrease in Rs followed by a quick reversion to a higher value indicates fast folding and tumbling of the PE. The periodicity in tumbling is evident from the peak in the power spectrum $P(\omega)$ of Rs shown in Fig. 4. As can be seen from Fig. 5, inclusion of the hydrodynamic interactions does not change this behavior qualitatively. But HI shifts the peak in the power spectrum to higher frequencies, indicating more frequent tumbling of the polymer. As we can see from Fig. 2, this tumbling through folding of the PE is quite different from tumbling of a rod in a shear flow. In addition we obtain the tumbling time by following the orientation of the end to end vector.[35] We see that the tumbling time obtained from this method matches well with the peak position of the power spectrum. The dependence of the tumbling time on the Peclet number Pe is shown in Fig. 6. Inclusion of the hydrodynamic interactions does not change this dependence of tumbling time on Pe but decreases its value, in correspondence with the increase in tumbling frequency. It is shown in Fig. 6 that the average width of the PE in the gradient direction R_{gz} and the tumbling time $\tilde{t}_t$ follows a power law scaling $R_{gz} \sim Pe^{-(1-m)/5}$ and $\tilde{t}_t \sim Pe^{-(1-m)4/5}$, with $m = 0.06$ obtained from the scaling of its width in the flow direction $R_{gx} \sim Pe^m$. This indicates that we are in a regime wherein the width R_{gz} is only limited by the time taken for the transverse protrusions to reach the end of the polymer.[10,35]

At higher shear rates R_{gz} exhibits significant deviation from the $-(1 - m)/5$ line and appears to follow the $Pe^{-1/4}$ rule suggested in Ref. 35, for transverse diffusion restricted by convection. But more data, at higher shear rates, are required to conclusively establish the mechanism for tumbling and distinguish it from the $\tilde{t}_t \sim Pe^{-2/3}$ scaling suggested in Ref. 36.

In the low electrostatic coupling regime, for $A < 5$, the dynamics of a PE under shear has similarities with that of a semiflexible polymer. This is expected, as the number of CCIs on the PE in this regime is low, the electrostatic repulsion between bare backbone charges induces a nonzero stiffness to the polymer. The periodic tumbling that we observe

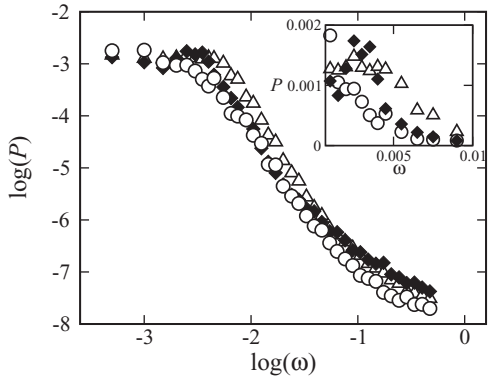

FIG. 4. Power spectrum of the extension $Rs(t)$ of an $N = 50$ BD-FD in a shear flow at $Wi = 20$, $A = 20$ (circles), $A = 10$ (triangles), and $A = 2$ (diamonds). The peak for $A = 2$ implies periodic tumbling. Inset shows the region around the peak in the power spectrum on a linear scale.

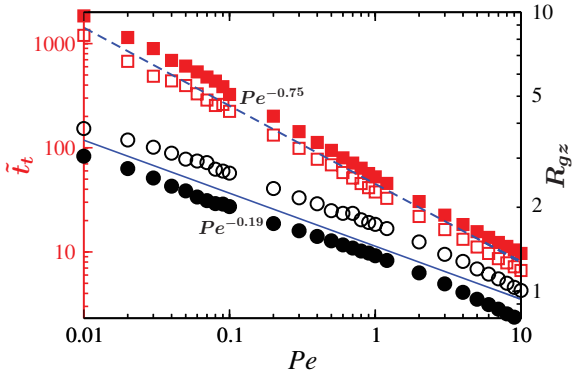

FIG. 6. Tumbling time $\tilde{t}_t$ and the width of the PE in the shear gradient directions R_{gz} as a function of the Peclet number Pe for a PE with $N = 50$ and $A = 2$. Open squares are for the BD-HI and filled squares are for the BD-FD model.

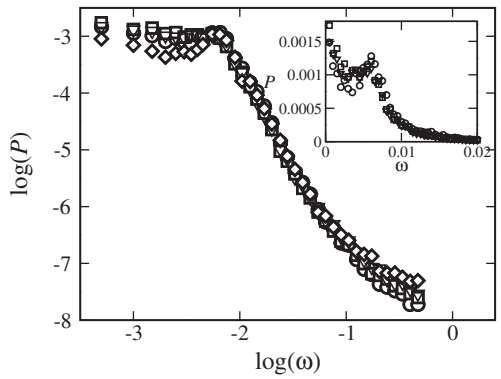

FIG. 7. Comparison of the power spectra of extension Rs, between PE and stiff neutral polymers, in a shear flow with $Pe = 0.5$ in the absence of HI. BD-FD with $N = 50$ and $A = 2$ (diamonds), neutral semiflexible polymer with bending rigidity $K_3 = 50$ (circles), $K_3 = 10$ (squares), and $K_3 = 5$ (triangles) is shown. Inset shows the region around the peak for three different values of K_3 of the neutral polymer.

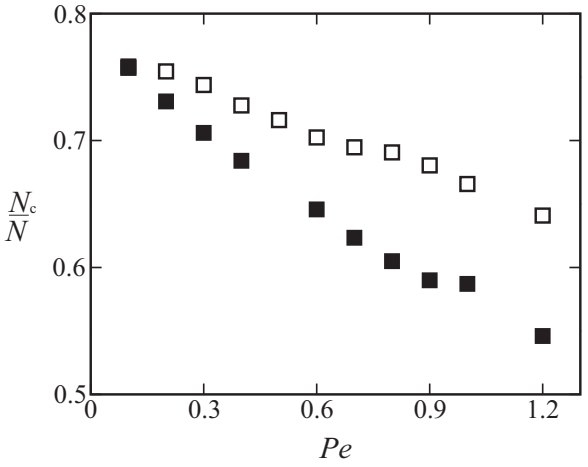

FIG. 8. The averaged fraction of condensed CIs on a PE with $N = 50$, $A = 5$ as a function of Peclet number, for BD-HI (open squares) and BD-FD (filled squares). A CI is considered as condensed when its distance from any of the monomer is less than or equal to $2b$.

for this range of A values is very similar to that was reported earlier for semiflexible polymers.[12] In their study, on the dynamics of semiflexible polymers in a shear flow, Munk *et al.* stressed on the importance of inextensibility criteria for obtaining periodic tumbling.[12] However, we see that inextensibility is not an essential criteria for periodic tumbling of polymers. To make a more quantitative comparison of our results with those of stiff neutral filaments, and to establish that the stiffness induced by the electrostatic repulsion leads to the periodic tumbling, we simulated a neutral bead-spring polymer chain with stiffness, incorporated through an angle potential $K_3(1 - \tilde{\mathbf{r}}_{ij} \cdot \tilde{\mathbf{r}}_{jk}/(\tilde{r}_{ij}\tilde{r}_{jk}))$ for each set of beads connected in the order (i, j, k). We find that the configurations obtained, for a stiff neutral polymer under shear, are similar to those for a PE shown in Fig. 2 (top panel). In Fig. 7, we compare the power spectrum of this stiff neutral polymer, obtained from its extension Rs in the direction of flow, for $K_3 = 5$, 10, 50 with that of a "flexible" PE at $A = 2$. As can be seen from this figure, for a given shear rate Pe, the power spectra of the neutral polymer of a certain stiffness matches well with that of a PE. One can also see that (inset of Fig. 7) the tumbling frequency is much better defined for larger value of stiffness K_3 and the peak is more diffused for low K_3 values.

As the coupling constant is increased to $A = 5$, we are in the regime where the average equilibrium configuration (i.e., in the absence of shear) is sausage like.[19,20] However, under shear, there is a decrease in the number of CCIs leading to the PE dynamics similar to that for $A = 2$. We must remember that, in the absence of shear, the fluctuations of a PE are most dominant around $A \sim 5$ and there is a strong anti-correlation between the number of CCIs and the extension of the PE.[19] In this regime the average number of CCIs depends strongly on the shear rate. For a given shear rate the number of CCIs is larger when the HI is included. In Fig. 8 we show the number of CCIs as a function of the shear rate with and without the HI. Note that the number of CCIs decreases with increase in the shear rate. This also means, since the relaxation time of the PE depends on the number of CCIs, that it is difficult to estimate the Wi in this regime. As in the equilibrium case, here we again see a strong anti-correlation between the number of CCIs and the extension of the PE in flow direction (see Fig. 9). The major difference between the condensed counterion fluctuation with and without the shear is that, in equilibrium the fluctuations in the radius of gyration of the polymer are driven by CI condensation fluctuations, while in the presence of shear, it is the shear induced structure of the PE, the periodic folding as it tumbles, that determines the counterion condensation. Like in the case of $A = 2$, here too the power spectrum of Rs shows a clear peak indicating periodic tumbling with a shift in peak to higher frequencies when the HI is included (data not shown).

For $A \approx 10$, in the absence of shear all the counterions are condensed and the equilibrium PE is in the collapsed globular state (see Fig. 1). Inclusion of the hydrodynamic interactions now qualitatively changes the behavior of a PE under shear in this regime. Let us first look at the case of $A = 10$, here the equilibrium configuration is collapsed globular, which when sheared extends and tumbles, with the shear induced CI fluctuations still playing a major role. For the FD case, the dynamics is similar to that for $A = 5$, with most of

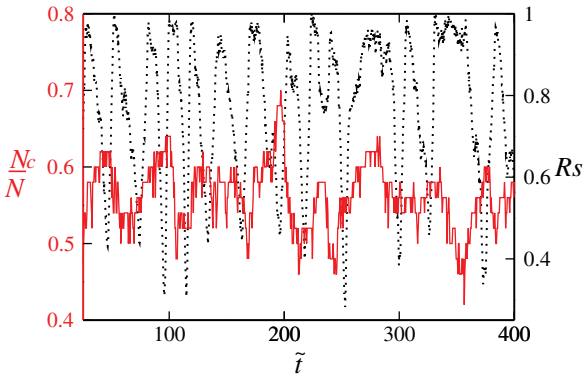

FIG. 9. Extension (dotted line) of an $N = 50$, $A = 5$, BD-FD, and the fraction of its condensed CIs (solid line) in a shear flow at $Pe = 1.2$. Similar relation holds for BD-HI also, but with smaller timescales for the fluctuation in condensed CIs.

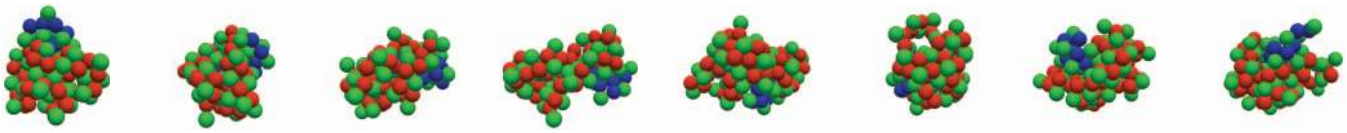

FIG. 10. Typical snapshots of an $N = 50$, $A = 20$ BD-HI in a shear flow at $Wi = 20$ at $\tilde{t} = 0.5$, $\tilde{t} = 2$, $\tilde{t} = 4$, $\tilde{t} = 6$, $\tilde{t} = 8$, $\tilde{t} = 10$, $\tilde{t} = 12$, and $\tilde{t} = 14$. The monomers are shown in red color and the condensed counterions are shown in green color. The relative position of the marked bead (blue color) demonstrates the tumbling of the PE.

the time spent in the extended state. The tumbling is again through folded configurations, but now the two strands of the fold remain bridged by the counterions as they slide against each other (see middle panel in Fig. 2). This is unlike that in equilibrium, where the PE configurations at $A = 5$ and $A = 10$ are distinctly different.[19] The power spectrum, shown in Fig. 4, still has a small peak implying weak periodicity in tumbling. On inclusion of the HI, the number of CCIs is higher and the collapsed structure is more favored. However, the PE occasionally extends as a whole and tumbles. The fluctuation of the number of CCIs makes the tumbling of PE aperiodic, with randomly distributed residence time at collapsed state. The aperiodicity in tumbling of BD-HI was also verified by calculating the PSD of orientation of the end to end vector. Thus, $A = 10$ is a special point, with the BD-FD remaining most of the time at the partially extended or fully extended state and the BD-HI staying at the collapsed state. As stated earlier the number of CCIs is a decreasing function of shear rate. As the number of CCIs decreases the time spend by the PE in its extended state also goes up.

B. Large electrostatic coupling, $A > 10$

For $A > 10$ the equilibrium configuration remains to be collapsed globular. Here inclusion of the HI qualitatively changes the dynamics under shear, as is evident from a comparison between the bottom panel of Fig. 2 and Fig. 10. As shown in Fig. 11, there is a critical shear rate above which the average extension of the PE as a function of the Wi shows a significant increase. The critical shear is higher in the presence of the HI. In the FD case the extension and tumbling are aperiodic and no peak is seen in the power spectrum (see Fig. 4). When HI is included, i.e., for the BD-HI, the PE extends only partially and tumbles periodically which is seen as a peak in the power spectrum (Fig. 12). The tumbling of this collapsed structure is shown in Fig. 10. Some monomers are colored differently to show the relative position of those as a function of time.

In all cases, the power spectrum of Rs exhibits a power law behavior at high frequencies. This is similar to the power spectrum of the extension of a Hookean dumbbell in simple shear, which is given by $P(\omega) \approx \dot{\gamma}^2\mu_0^2/(\kappa^2+\omega^2)^2 + 1.0/(\kappa^2+\omega^2)$,[10] here κ is the spring constant scaled by the viscous drag coefficient or the inverse of the Hookean relaxation time of the spring; μ_0 is the self mobility of the dumbbell beads. When $(\kappa^2+\omega^2) < \dot{\gamma}^2$, the PSD decays as ω^{-4}, while for $(\kappa^2+\omega^2) > \dot{\gamma}^2$ the second term is more dominant and the PSD decays as ω^{-2}. The power spectrum of the PE fits well to that for a dumbbell except in the region near the periodic tumbling frequency. We use this fact to calculate an effective spring constant or the relaxation time of the PE as a function of Peclet number. The results from this analysis are shown in Fig. 13.

We also calculate the tumbling time by following the orientation of the end to end vector at higher shear rates and orientation of the monomers with respect to the polymer center of mass at lower shear rates.[35] The change in the dynamics of PE on inclusion of HI is again evident from the data presented in Fig. 14. At lower shear rates, BD-HI data show a power law dependence of tumbling time as a function of Pe with an exponent ~ -1.0, while the widths in the flow and the gradient directions having only a weak dependence on Pe. Periodicity of tumbling is evident from the sharply peaked distribution of tumbling times shown for $Pe = 1.2$. We see similar distribution of tumbling time for all values of $Pe < 2.0$. The tumbling time dependence of Pe in this regime does not fit into any that was reported earlier for neutral polymers.[10,35,36] As is evident

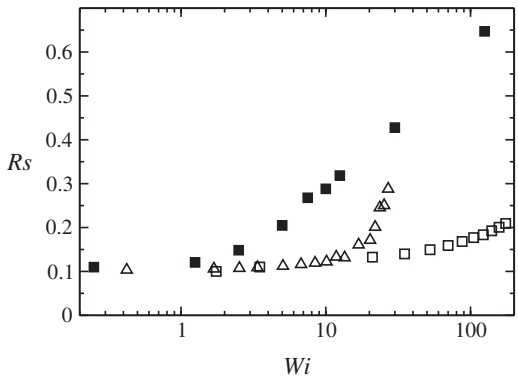

FIG. 11. Comparison of average extension of an $N = 50$, $A = 20$ BD-FD (filled squares), BD-HI (open squares), and from DPD (triangles), in a shear flow as a function of Wi.

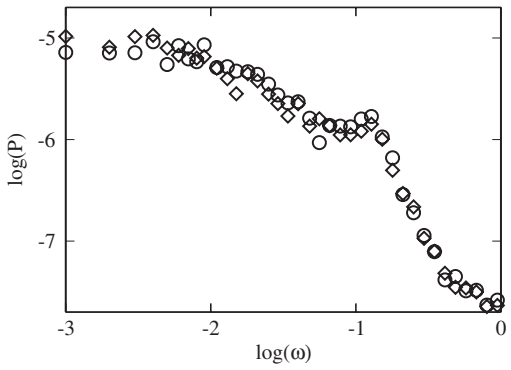

FIG. 12. Power spectrum of the extension Rs of an $N = 50$, $A = 20$ BD-HI in a shear flow at $Wi = 20$, in the presence of hard boundary in the shear gradient direction (open diamonds) and with Lees-Edwards boundary condition in the shear gradient direction (open circles).

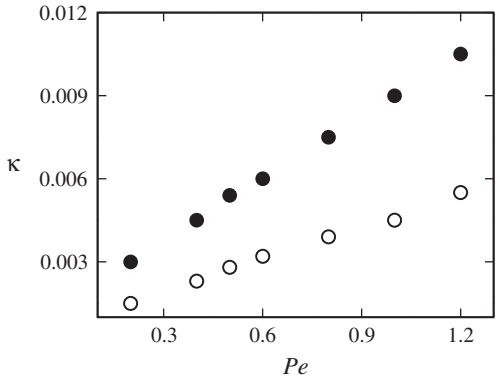

FIG. 13. Effective spring constant of an $A = 10$ BD-FD in a shear flow as a function of Pe, for N = 100 (open circles) and N = 50 (filled circles).

from Fig. 10, where the snapshots of the PE over one tumbling event are shown, the tumbling here involves very little deformation of the collapsed structure, but follows a similar pattern as the dumbbell tumbling model described in Ref. 37. However, we do not see the ratio of the fractional thickness in the gradient direction to the mean fractional extension in the flow direction showing any power law dependence on shear rate. For small shear rates this ratio remains constant at unity and the tumbling time scales as Pe^{-1}. As the shear rate increases this ratio of widths decreases, but absence of any simple power law behavior here makes it intractable for further analysis. In the BD-FD case, we do not observe any power law scaling of t_t, R_{gx}, R_{gz} as a function of Pe. The distribution of the tumbling time is broad, indicating absence of any dominant periodic modes, which agrees with the absence of any peak in the PSD of Rs.

In order to verify that the nature of the boundary conditions has no specific role, we have carried out the simulations using two possible shear boundary conditions. In Fig. 12, the power spectrum of the extension of a PE in the presence of the HI, for different boundary conditions, is presented. It is found that, for the box size, which we used for the simulations, different boundary conditions have negligible effect on the dynamics of the PE. It should also be mentioned that the mobility matrix used in the present work is not expected to be accurate when the local density of beads is high.[30,31] In addition there will be multi-particle effects which we neglect. We therefore expect some change in the counterion distribution at high coupling regime when the solvent is treated explicitly. This issue will be addressed again in Sec. IV.

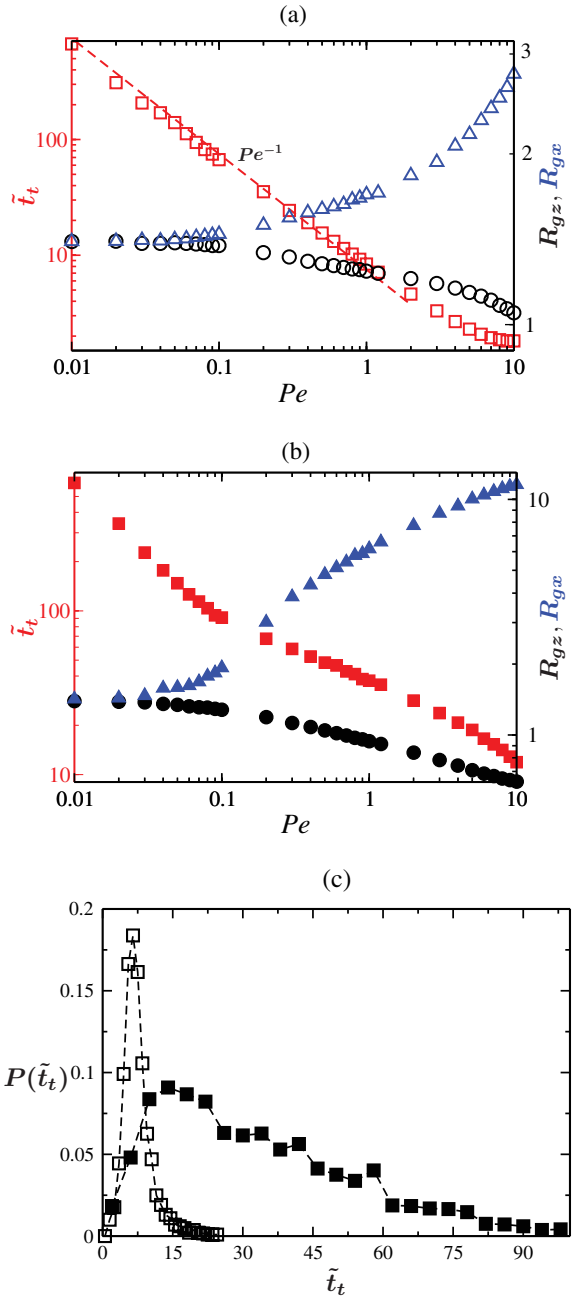

FIG. 14. Tumbling time $\tilde{t}_t$ and the width of the PE in the shear gradient R_{gz} and the flow R_{gx} directions, as a function of the Peclet number Pe with $N = 50$ and $A = 20$ for BD-HI (a) and BD-FD (b). (c) Comparison of the distribution of tumbling time at $Pe = 1.2$, for BD-HI (open squares) and BD-FD (filled squares).

IV. COMPARISON WITH DPD SIMULATIONS

We have so far assumed instant propagation of the solvent mediated forces, neglected near field solvent effects, and assumed minimum image boundary conditions for the electrostatic interactions. In this section we will see what effect does these assumptions have on the results presented so far. To achieve this we use an explicit solvent model and use the DPD thermostat to preserve hydrodynamic interactions. We switch to three-dimensional periodic boundary conditions and use Ewald summation for calculating electrostatic interactions. DPD is known to correctly reproduce long range hydrodynamic interactions, though the effects due to finite propagation time of fluid mediated forces will be exaggerated. We therefore expect the hydrodynamics propagation time to be over estimated in DPD compared to that in real fluids, with the true propagation time somewhere in between that in DPD and BD. We will come back to this point later. Long range electrostatic interactions are now included via Ewald summation.

In the DPD simulations the monomer-monomer interactions and the monomer-CI interactions are kept the same as described earlier for BD simulations. The solvent is

represented by DPD beads interacting through soft repulsive pairwise forces described in Sec. II B. The monomer-solvent and CI-solvent interactions, are set to be the same as that between solvent particles. These interactions ensure that, in the absence of electrostatic forces, the polymer is in a good solvent condition. Shear rate is imposed by Lees-Edwards boundary conditions in the shear gradient direction and periodic boundary in the other two directions.

DPD simulations are considerably more expensive computationally than BD. We therefore restrict our comparison study to the regime with $A = 20$ where we saw dramatic difference in the dynamics of the PE when HI were included. A more detailed study covering all values of A will be published elsewhere.

A. Time scales in DPD and BD

To make a comparison between the results obtained from DPD and BD we need to normalize the characteristic time scales in these two methods. In polymer simulations there are two different time scales, one is monomer diffusion time (τ) and the other is polymer relaxation time (τ_R). As described earlier the monomer relaxation times in DPD and BD are labelled as τ_{DPD} and τ_{BD}, respectively. The dimensionless numbers, Peclet number and Weissenberg number, are then given by the following relations:

$$\begin{aligned} Pe &= \dot{\gamma}\tau, \\ Wi &= \dot{\gamma}\tau_R. \end{aligned} \tag{15}$$

The polymer relaxation time (τ_R) can be calculated from the correlation of the equilibrium end to end distance. For a given electrostatic coupling constant, τ_R is different in DPD and BD. For the coupling constant $A = 20$, the τ_R in DPD is $84.3\,\tau_{DPD}$ and in BD it is $17.5\,\tau_{BD}$. To compare the time series of polymer extension between BD and DPD, we used the dimensionless time (τ/τ_R), i.e, DPD simulation results are given in units of $\tau_{DPD}/\tau_{R(DPD)}$ and that of BD are in units of $\tau_{BD}/\tau_{R(BD)}$.

B. Electrostatics

We compare the PE extension in the direction of shear obtained from DPD simulations with the electrostatic interactions calculated using minimum image boundary conditions and that with Ewald sum. Typical results obtained from these simulations are shown in Fig. 15. From the time series of extension in the direction of shear and its histogram we can conclude that inclusion of Ewald summation has not changed the trajectory of the polymer appreciably. In fact, we find that the average properties of the polymer, obtained with and without the Ewald summation, are exactly the same.

C. Critical shear rate

We had earlier seen, from the BD simulations, that at $A = 20$ the critical shear rate required to open up the PE is larger when hydrodynamic interactions are included. Corresponding increase in the number of condensed counterions was also noticed on inclusion of HI. To illustrate how the presence of explicit solvent modifies these results we compared the time series of polymer extension, obtained from DPD and BD simulations for a fixed value of $A = 20$ and $Wi = 20$. At this shear rate and electrostatic coupling strength, BD simulations showed no PE extension events. By contrast, extension of the PE is quite frequent in DPD simulations, indicating that critical shear rate is lower in the DPD simulations. From Fig. 11 we see that the critical shear rate in DPD simulations is in between that for BD-FD and BD-HI simulations. It is interesting to see that the critical shear rate is larger with BD-HI and that the extension rises much more sharply. These results are similar to that seen in the case of neutral polymers.[17]

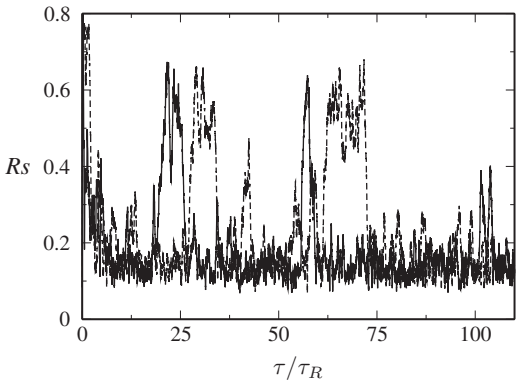

FIG. 15. Comparison of the PE extension in a shear flow, obtained using two different methods to calculate the electrostatic forces, with $Wi = 20$, $A = 20$, and $N = 50$. Solid lines are with Ewald sum and dashed lines are with minimum image boundary condition.

D. Number of condensed counterions and power spectrum of extension

As stated earlier the number of condensed counterions, for a fixed electrostatic coupling constant, decreases with the shear rate and is higher when hydrodynamic interaction is included, as HI modifies the local flow profile (see Fig. 16). The apparent coupling of counterions to the PE is much stronger with BD-HI and necessitates higher shear rate to extend the PE.

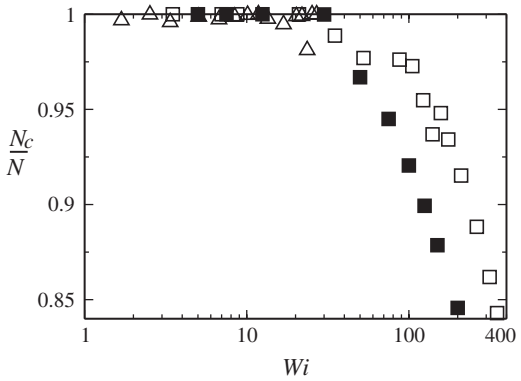

FIG. 16. Comparison of the averaged fraction of CIs on a PE with $N = 50$ and $A = 20$ as a function of Wi, for BD-HI (open squares), BD-FD (filled squares), and DPD (open triangles).

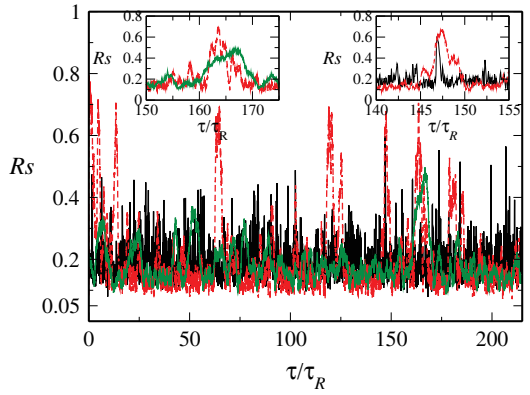

FIG. 17. Comparison of the PE extension with same average extension in BD-HI (black), BD-FD (green), and DPD (red) with $Rs = 0.2$, $A = 20$, and $N = 50$. Inset shows an enlarged view of single extension events.

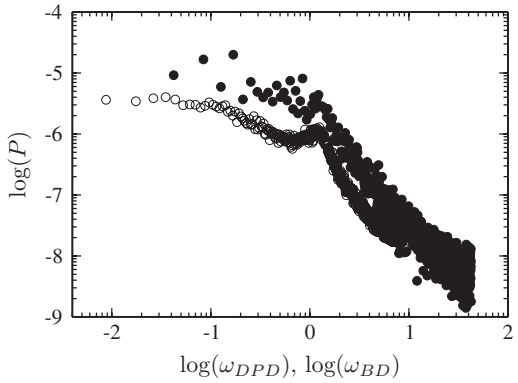

FIG. 18. Comparison of the power spectrum of the extension Rs of a PE with $N = 50$ at $A = 20$ between BD-HI (open circles) at $Wi = 20$ and DPD (filled circles) simulations at $Wi = 10$.

E. Dynamics of extension

Not only the average extension, but also the dynamics of opening and folding are dependent on the nature of hydrodynamic interaction. This is evident from the comparison of time series of extension, for the same average extension, obtained by choosing $Wi = 22$ for DPD, $Wi = 157.5$ for the BD-HI, and 3.5 for BD-FD simulations. From Fig. 17, we see that while DPD simulations show smaller number of large extensions, the same average extension is obtained in BD due to more frequent small extensions of the polymer. We also see that the extension events are broader when the hydrodynamic propagation time is slower, with BD-HI being the most narrow and the BD-FD the broadest. This is coupled to the fact that, in the free draining limit, we see more counterions being detached from the PE during its extension increasing repulsion between monomers. Similarly, as shown in Fig. 18, their power spectra of extension at the same average extension are not exactly the same. The periodic tumbling seen for BD-HI, which manifests as a peak in the power spectra, is less pronounced in DPD simulations, even though their time series and snapshot sequences *look* similar (data not shown). It will be interesting to see these effects by systematically modifying Schmidt number, *Sc*. However, it is not possible to alter Sc in DPD by orders of magnitude.[41] A systematic study of the dependence of critical shear rate on Sc can be carried out using Lowe-Anderson thermostat,[42] this work is in progress and the results will be published elsewhere.

In summary, the simulations using DPD thermostat and Ewald sum for electrostatic interactions show that, at high electrostatic coupling, the periodic minimum image boundary condition is sufficient to incorporate the electrostatic forces correctly. It is evident that the critical shear rate required to extend the PE is the largest for BD-HI, the smallest for BD-FD, and that obtained from DPD is in between these two. This indicates that hydrodynamic interactions, which are different in these three simulations, play an important role in determining the dynamics of PE. The differences in hydrodynamic interactions can be characterized by three parameters, Reynolds number (*Re*), Schmidt number (*Sc*), and the hydrodynamic interaction parameter (h^*). In our simulations the parameter h^* is same. In DPD, $Sc \sim 1$ which is much lower than real systems, which would indicate an unrealistically large momentum propagation time compared to mass diffusion. However, the amount by which a particle may have moved, within the time momentum has propagated through the solvent to the farthest end of the polymer blob, is the factor which is important here. Given that the radius of gyration of the polymer, R_g, and the shear rates are the same in DPD and BD-HI simulations, this propagation time will be proportional to *Re*. *Re* in our DPD simulation is of the order 10 while $Re = 0$ in BD-HI simulations. Given that in typical experimental situations *Re* is of the order 10^{-7}, BD-HI results should be closer to experiments than DPD.

V. CONCLUSION

In this paper we have analyzed the dynamics of a polyelectrolyte in simple shear flow, taking into account the CI dynamics explicitly, for different values of the electrostatic coupling constant *A* and at different shear rates. Periodicity in the tumbling of the PE was investigated using time series of end to end vector orientation and extension in the direction of flow. Periodic tumbling of the PE is observed at lower coupling constants, wherein the number of CCIs is very low at all times. At higher values of *A*, the CI fluctuations make the tumbling aperiodic and periodicity is obtained only when the HI suppress condensed CI fluctuations. In all cases, at high frequencies, the power spectrum of extension exhibits a power law, similar to that for a dumbbell in shear flow. The dynamics at low *A* is similar to that of a semiflexible polymer as the number of condensed CIs is low and the repulsion between monomers induces stiffness. At high *A* the dynamics changes qualitatively on the inclusion of hydrodynamic interactions and the increase in shear rates. We find that the hydrodynamic interactions have the effect of reducing the condensed CI fluctuations and also increasing the number of condensed CIs for a given shear rate. This leads to strong dipolar attractive interactions between the monomer-CI pairs pushing the critical shear rate for extension to very high values. The tumbling dynamics of the PE for the BD-HI, below this critical shear rate, is similar to that of a dumbbell stretch-align-flip-collapse mechanism. In general, larger CI fluctuations lead to dynamics that is qualitatively different from that of

neutral polymers with aperiodic extension and tumbling events, which are most prevalent in the regime where there is a moderate number of CCIs.

To check for the influence of boundary conditions and truncation of the electrostatic interactions used, the results obtained from BD simulations are compared with that from DPD simulations, for $A = 20$, with fully periodic boundary conditions and Ewald summation for electrostatic interactions. We show that inclusion of Ewald summation does not change the results. Our results also indicate that stronger coupling of the CIs with the PE resulting from stronger hydrodynamic interactions leads to a distinctly different PE dynamics.

We find that the PE dynamics is strongly coupled to the dynamics of CIs. We show that, since the number of condensed CIs has a strong dependence on the value of A and the shear rate, the tumbling behavior of PE changes drastically as these parameters are varied. DNA would be an ideal experimental system to investigate this interesting and rich behavior of PE. Unfortunately from the experimental data available in the literature it is not clear in what regime of electrostatic coupling they were carried out and what is the role of the CIs. Experiments using large CIs, which could be achieved by replacing the small atomic CIs with larger molecular ions, could be better suited for comparison with the simulation results presented here. On the simulation side also more systematic analysis is required to see the mechanism of tumbling and extension at high and intermediate A values. It may be interesting to see how presence of multivalent ions and salt changes the dynamics as they could connect to experiments more easily. Our future work will focus more on these directions.

ACKNOWLEDGMENTS

The simulations were carried out at the High Performance Computing Environment at IIT Madras.

[1]M. Chopra and R. G. Larson, J. Rheol. **46**, 831 (2002).
[2]R. G. Larson, J. Rheol. **49**, 1 (2005).
[3]F. Oosawa, *Polyelectrolytes* (Marcel Dekker, New York, 1971).
[4]R. R. Netz and D. Andelman, Phys. Rep. **380**, 1 (2003).
[5]R. Schiessel and P. Pincus, Macromolecules **31**, 7953 (1998).
[6]C. Stoltz, J. J. de Pablo, and M. D. Grahamb, J. Chem. Phys. **126**, 124906 (2007).
[7]A. Pamies, J. G. H. Cifre, and J. G. de La Torre, J. Polym. Sci., Part B: Polym. Phys. **45**, 1 (2007).
[8]D. E. Smith, H. P. Babcock, and S. Chu, Science **283**, 1724 (1999).
[9]P. LeDuc, C. Haber, G. Bao, and D. Wirtz, Nature (London) **399**, 564 (1999).
[10]J. S. Hur, E. S. G. Shaqfeh, and R. G. Larson, J. Rhoel. **44**, 713 (2000).
[11]C. M. Schroeder, R. E. Teixeira, E. S. G. Shaqfeh, and S. Chu, Phys. Rev. Lett. **95**, 018301 (2005).
[12]T. Munk, O. Hallatschek, C. H. Wiggins, and E. Frey, Phys. Rev. E **74**, 041911 (2006).
[13]P. Szymczak and M. Cieplak, J. Chem. Phys. **127**, 155106 (2007).
[14]S. W. Schneider *et al.*, Proc. Natl. Acad. Sci. U.S.A. **104**, 7899 (2007).
[15]A. Alexander-Katz *et al.*, Phys. Rev. Lett. **97**, 138101 (2006).
[16]A. Alexander-Katz and R. R. Netz, Europhys. Lett. **80**, 18001 (2007).
[17]A. Alexander-Katz and R. R. Netz, Macromolecules **41**, 3363 (2008).
[18]N. Hoda and S. Kumar, J. Chem. Phys. **127**, 234902 (2007).
[19]K. Jayasree, P. Ranjith, M. Rao, and P. B. S. Kumar, J. Chem. Phys. **130**, 094901 (2009).
[20]H. J. Limbach and C. Holm, J. Phys. Chem. B **107**, 8041 (2003).
[21]A. W. Lees and S. F. Edwards, J. Phys. C **5**, 1921 (1972).
[22]G. C. Ansell and E. Dickinson, J. Colloid Interface Sci. **110**, 73 (1986).
[23]J. K. G. Dhont, *An Introduction to Dynamics of Colloids* (Elsevier, Amsterdam, 1996).
[24]J. Rotne and S. Prager, J. Chem. Phys. **50**, 4831 (1969).
[25]J. R. Blake, Proc. Cambridge Philos. Soc. **70**, 303 (1971).
[26]Y. W. Kim and R. R. Netz, J. Chem. Phys. **124**, 114709 (2006).
[27]M. Doi and S. F. Edwards, *The Theory of Polymer Dynamics* (Claredon Press, Oxford, 1994).
[28]R. M. Jendrejack, M. D. Graham, and J. J. de Pablo, J. Chem. Phys. **113**, 2894 (2000).
[29]D. L. Ermak and J. A. McCammon, J. Chem. Phys. **69**, 1352 (1978).
[30]C. W. J. Beenakker and P. Mazur, Physica A **126**, 349 (1984).
[31]G. Bossis and J. F. Brady, J. Chem. Phys. **87**, 5437 (1987).
[32]R. R. Netz, Phys. Rev. Lett. **90**, 128104 (2003).
[33]H. Wada, Y. Murayama, and M. Sano, Phys. Rev. E **72**, 041803 (2005).
[34]S. Plimpton, J. Comput. Phys. **117**, 1 (1995).
[35]I. S. Dalal, A. Albaugh, N. Hoda, and R. G. Larson, Macromolecules **45**, 9493 (2012).
[36]J. S. Lee, E. S. G. Shaqfeh, and S. J. Muller, Phys. Rev. E **75**, 040802(R) (2007).
[37]R. E. Teixeira, H. P. Babcock, E. S. G. Shaqfeh, and S. Chu, Macromolecules **38**, 581 (2005).
[38]P. J. Hoogerbrugge and J. M. V. A. Koelman, Europhys. Lett. **19**, 155 (1992).
[39]P. Espagnol and P. Warren, Europhys. Lett. **30**, 191 (1995).
[40]P. Espagnol, Europhys. Lett. **40**, 631 (1997).
[41]X. Fan, N. Phan-Thien, S. Chen, X. Wu, and T. Y. Ng, Phys. Fluids **18**, 063102 (2006).
[42]K. R. Prathyusha and P. B. S. Kumar, in *Proceedings of the ATIP/A*CRC Workshop-2012* (A* STAR Computational Resource Center, 2012), p. 124.